Effects of Charge State on the Structures of Serum Albumin Ions in the Gas Phase: Insights from Cation-to-Anion Proton-Transfer Reactions, Ion Mobility, and Mass Spectrometry

Meagan M. Gadzuk-Shea, Matthew F. Bush*

jp-2018-084278 submitted to *J. Phys. Chem. B* on August 29, 2018

Revised manuscript submitted on October 10, 2018

Contribution from the:

University of Washington, Department of Chemistry, Box 351700

Seattle, WA 98195-1700

*Email: mattbush@uw.edu

Abstract

Understanding the structures of proteins in the gas phase is essential for using gas-phase measurements to infer the properties of proteins in solution. Using serum albumin as a model, this study aims to expand our understanding of this relationship for a larger (66 kDa), multi-domain protein that contains 17 internal disulfide bonds. Gas-phase ions were generated from five solutions that preserve varying extents of native structure. Ion mobility (IM) mass spectrometry (MS), cation-to-anion proton-transfer-reactions (CAPTR), and energy-dependent IM were used to probe the relationship between structure, charge, and solution. Ions generated from increasingly disruptive conditions exhibited higher charge states and larger collision cross section values. The collision cross sections of all CAPTR products depend on the original solution, and to varying extents, the charge state of the product and the precursor. For example, the collision cross sections of CAPTR products from denaturing conditions are all significantly larger than those of the original native-like ions. Results from energy-dependent experiments show that the structures of the original ions from electrospray ionization and their CAPTR products are a consequence of kinetic trapping and depend on the higher-order structure and disulfide bonding of serum albumin in solution. This study builds on our understanding of the relationship between solution condition, disulfide bonding, collision cross section, and charge for a larger, multi-domain protein, which may be applicable to future characterization of biotherapeutics that share these structural features.

Introduction

The biological functions and activities of proteins depend inextricably on their higher-order structures.[1] With a detailed understanding of this relationship, it is possible to tailor the function of a protein by manipulating its stability, conformational distribution, solubility, and assembly.[2–4] This concept has been applied in therapeutic research and development. For example, knowledge of the insulin dimerization interface was exploited to introduce single amino acid substitutions that cause like-charge repulsion at the interface.[5] These substitutions do not disrupt the receptor binding region of the functional monomer, but reduce the fraction of total insulin that forms lower-activity dimers at clinical concentrations.[5,6] This dramatically decreases the food-related, time sensitivity of insulin intake for diabetic patients. Despite this and other successes,[6,7] our ability to study the dynamics, evolution, and characteristics of a protein structure remains hindered. Condensed-phase techniques play dominant roles in structural biology and biophysics,[8] but possess inherent limitations. These techniques convolve intra- and intermolecular forces, are hindered by the presence heterogeneous mixtures of structure,[9] and often require that proteins are amenable to high concentrations and/or crystallization. Such challenges restrict the proteins that may be studied by condensed-phase techniques.[10]

The study of "naked" proteins in the solvent-free environment of a mass spectrometer isolates the intrinsic, intramolecular interactions by eliminating interactions with solvent and surrounding molecules. Furthermore, mass spectrometry (MS) offers rapid analysis, requires small amounts of sample, and is applicable to many more proteins relative to conventional techniques.[11] MS has been used to determine the mass,[12,13] connectivity,[14] interactions,[15] and stoichiometry[16,17] of proteins and protein complexes. Ion mobility (IM) has emerged as a useful technique to couple with MS and provides a complementary dimension of analysis that is

sensitive to shape and size.[18] This structural information is obtained by measuring the mobility of an ion in a buffer gas under an electric field, which can be converted to a collision cross section (Ω).[19]

Electrospray ionization from "native-like" solutions (*i.e.*, aqueous solutions with ionic strength and pH similar to physiological conditions) can yield protein ions with Ω values that are correlated with those calculated based on condensed-phase structures.[20,21] The evolution of native MS and the study of protein structure in the gas-phase have been reviewed previously.[22,23] There is substantial evidence that native-like ions can retain additional properties of their condensed-phase counterparts. For example, hybrid IM, infrared action spectroscopy, and MS analysis of native-like ions of β-lactoglobulin and myoglobin yielded infrared signatures that were consistent with the expected degrees of β-sheet and helical composition in solution.[24] Additionally, ions of the endospores of *Bacillus subtilis* have been successfully cultured following high-velocity collisions with surfaces, demonstrating that protein ions from electrospray ionization can even maintain biological function.[25]

Protein ions formed from denaturing solutions (*e.g.*, organic and acidified) exhibit higher charge-state (z) and Ω values than their native-like counterparts.[26,27] Interestingly, when these high-z ions undergo charge reduction in the gas phase, the resulting charge-reduced product ions can have more compact Ω values than the initial, unreduced ions.[28–31] The extents of charge reduction that can be achieved using ion/neutral reactions are limited by the thermodynamics and kinetics of those reactions.[32] Charge-transfer reactions between cations and anions are exothermic even at low charge states[33] and can proceed through either electron-transfer (Reaction 1) or proton-transfer reactions (Reaction 2):

$$[M_n+xH]^{x+}+A^{\bullet -} \rightarrow [M_n+xH]^{\bullet (x-1)+}+A \rightarrow \text{Dissociation} \qquad \text{Reaction (1)}$$

$$[M_n+xH]^{x+} + A^- \rightarrow [M_n+(x-1)H]^{(x-1)+} + AH \qquad \text{Reaction (2)}$$

Electron transfer yields a radical cation, which can undergo subsequent bond cleavage and fragmentation, *i.e.*, electron-transfer dissociation (ETD).[34] Conversely, proton-transfer reactions produce even-electron products that do not spontaneously fragment, which enables analysis of charge-reduced molecular ions.[32,33]

Recently, we introduced cation-to-anion proton-transfer-reactions (CAPTR) as a method to produce many charge-reduced product ions from isolated precursor ions via Reaction 2.[35] We've developed a strategy for investigating the relationship between z, Ω, and original solution condition of proteins that uses CAPTR, IM, and MS.[30,36–38] For example, the Ω values of lysozyme ions generated from denaturing solution conditions are larger than those generated from native-like conditions. From denaturing conditions, lysozyme ions with four intact disulfide bonds have smaller Ω values than the corresponding ions with reduced disulfide bonds.[37,39] The CAPTR products of ions from both intact and reduced denaturing conditions all exhibit smaller Ω values than the respective precursor ions. Interestingly, for CAPTR products with $z \leq 6$, the disulfide-reduced products have smaller Ω values than corresponding disulfide-intact products. At the lowest z measured, all product ions isomerize to structures with Ω values similar to those measured for ions from native-like conditions and calculated from the crystal structure, although small differences were observed.[37] These results indicate that the structure and dynamics of gas-phase protein ions can depend on disulfide bonding and original condensed-phase environment. Other work has shown that for large protein and protein complex ions from native-like solutions (*i.e.*, aqueous 200 mM ammonium acetate at pH 7.0), the magnitude of excess charge can have small, but statistically significant, impacts on their Ω values.[38] These

findings emphasize the importance of considering charge when using IM-MS to study structure in the gas phase.[40]

Here, we use CAPTR, IM-MS, and post-CAPTR activation to characterize the structures of serum albumin ions in the gas phase. Serum albumin is a 66 kDa protein that contains 17 internal disulfide bonds and three domains. Ions were generated from multiple solution conditions that retain varying extents of the native structure. The objective of this study is to expand our understanding of the relationship between solution conditions, internal disulfide bonds, Ω, and z for a larger, multi-domain protein.

Methods

Sample Preparation. Bovine serum albumin, which will be referred to as 'serum albumin', was purchased from Sigma Aldrich (St. Louis, MO) and prepared to a final protein concentration of 18-20 μM in each of the five solutions that are summarized in Table 1. For native-like, disulfide-intact (NI) conditions, the protein was dissolved in aqueous 200 mM ammonium acetate at pH 7.0. For native-like, disulfide-intact, supercharging conditions (NISC), 3% by volume sulfolane was added to the solution for NI conditions. For denatured, disulfide-intact (DI) conditions, the protein was dissolved in a 70:30 (v:v) mixture of ultrapure MilliPore water and methanol with 0.1% by volume trifluoroacetic acid. For denatured, disulfide-intact, supercharging (DISC) conditions, the protein was dissolved into an 84.5:15:0.5 (v:v) mixture of water, propylene carbonate, and glacial acetic acid. Serum albumin was also reduced and alkylated using a procedure described in the *Supporting Information* and then stored at −80° C until use. For denatured, disulfide-reduced, supercharging (DRSC) conditions, the disulfide-reduced sample was transferred using a Merck ZipTip pipette tip (Darmstadt, Germany) into a

1:1 (v:v) mixture of acetonitrile and water with 0.1% trifluoroacetic acid, to which 15% by volume propylene carbonate was added.

All experiments were conducted on a Waters Synapt G2 HDMS equipped with a glow-discharge ionization source for ion/ion chemistry[41] and a radio-frequency (rf) confining drift cell.[42] Cations were generated using nanoelectrospray ionization from borosilicate capillaries with inner diameters of 0.78 mm pulled to an ~1-3 μm tip using a Sutter Instruments P-97 micropipette puller (Novato, CA). A platinum wire was inserted into the wide end of the capillary to make electrical contact with the solution. The atmospheric-pressure interface was maintained at 120 °C, which has been shown to induce some heat transfer to the sample.[36] For CAPTR, perfluoro-1,3-dimethylcyclohexane (PDCH, Sigma Aldrich, St. Louis, MO) vapor[32] was introduced into the glow-discharge ionization source.[41] The $[PDCH-F]^-$ fragments at m/z 381 were quadrupole selected and accumulated in the trap cell for 100 ms. The polarity of the instrument was then switched to positive mode and a narrow m/z window corresponding to a single charge state of the protein was quadrupole selected and transmitted through the cloud of accumulated anions for 2 to 10 s to induce CAPTR.[35] Charge-reduced product ions and residual precursor ions were then pulsed into the mobility cell for 200 μs every 27.6 or 36.4 ms, depending on the maximum m/z measured. Representative mass spectra are shown in Figure S1.

IM arrival-time distributions were measured using an rf-confining drift cell.[42] A constant electric field of 5 V cm^{-1} was applied to the drift cell, which was filled with approximately 1.4 Torr helium or 1.2 Torr nitrogen gas. Ω values and apparent widths were determined using a method reported previously[37] and described in the *Supporting Information*. Briefly, field-dependent measurements were used to determine the m/z-dependent and m/z-independent transport times of ions from the end of the mobility cell to the entrance of the time-of-flight mass

analyzer. The arrival-time distributions measured at a single field strength were corrected for these transport times and used to calculate mobility (K) distributions. These K distributions were then converted to apparent Ω distributions using the Mason-Schamp equation:[19]

$$\Omega = \frac{3ez}{16N}\left(\frac{2\pi}{\mu k_B T}\right)^{1/2}\frac{1}{K} \quad (3)$$

where z is the charge state, e is the elementary charge, N is the number density of the drift gas, μ is the reduced mass of the ion and the drift gas, k_B is the Boltzmann constant, and T is the temperature of the drift gas (301 K). For post-CAPTR activation experiments, ions were collisionally activated during injection into the mobility cell. Note that activation can induce some spontaneous loss of charge.[30]

Results and Discussion

Using serum albumin as a model, this study aims to expand our understanding of the relationship between solution conditions, internal disulfide bonds, Ω, and z for a larger, multi-domain protein. This protein was selected because many biotherapeutic also contain multiple domains and are stabilized by disulfide bonds. Serum albumin ions were generated from five conditions that retained varying degrees of the native structure and are summarized in Table 1. IM-MS of ions generated from each solution condition will be used to examine the relationship between Ω and z of the original ions from electrospray. CAPTR of selected ions from each condition will be used to build a more general understanding of the relationship of Ω and z. Finally, results from energy-dependent experiments of z = 15+ ions generated through three different pathways will be used to compare the structures and stabilities of these ions.

Serum Albumin Ions from Electrospray. Figure 1 shows representative mass spectra obtained from each condition. Figure S2 shows that the neutral mass of the ions from DRSC

conditions is ~2 kDa heavier than those from DISC conditions, which is consistent with the reduction and alkylation of the 17 native disulfide bonds and one free cysteine for the former. The maximum and minimum charges states observed from the spectra in Figure 1 are summarized in Table 1. Note that the range of charge states exhibited in a specific mass spectrum depends to some extent on the electrospray emitter and other parameters. The magnitude and widths of the charge state distributions exhibited by the ions generally increase with the increasingly disruptive nature of the solution condition (*i.e.*, NI < NISC < DI <DISC < DRSC). Results from mass spectrometry of serum albumin from various solution conditions (although not necessarily the exact same conditions used here) have been reported previously.[43,44] The values for the highest charge states observed for ions generated from DISC and DRSC conditions are generally consistent with those results, although some lower charge states observed previously were not observed in the present experiments. The charge-state distributions observed from NI, NISC, and DI conditions are consistent with previously reported values.[44,45]

The mobilities of all ions were determined by measuring the time for an ion to traverse an rf-confining drift cell containing helium gas,[42] as described in the *Methods*. The arrival-time distributions were converted to median collision cross section with helium ($\tilde{\Omega}$) values as described in the *Methods* section, and the resulting values for a subset of ions from each condition are shown in Figure 2. For the ions from NI, NISC, DI, DISC, and DRSC conditions, the $\tilde{\Omega}$ values ranged from 40.2 to 41.3 nm^2, 43.6 to 56.6 nm^2, 93.0 to 109.9 nm^2, 119.3 to 129.4 nm^2, and 141.6 to 158.7 nm^2, respectively. The $\tilde{\Omega}$ values of these ions depend strongly on the original solution conditions; notably, none of the $\tilde{\Omega}$ ranges overlap. Ω values were calculated for native, α-helical, and linear models of serum albumin, as described in the *Supporting*

Information and reported in Table S1. These models serve as qualitative points of comparison that are compact, extended with significant interactions between neighboring residues, and completely extended, respectively. Briefly, values measured for the NI ions are consistent with those calculated for the native model, values measured for the DRSC ions are between those calculated for the α-helical and linear models, and results for the ions from the other conditions fall between the two extremes. Additional comparisons between the experimental and calculated results are included in the *Supporting Information*. The $\tilde{\Omega}$ values from DI, NISC, and NI conditions are consistent with previous reports.[44,45] Ω_{N_2} values have been reported for serum albumin ions from conditions that are similar to the DISC and DRSC conditions used here, but directly comparing results from He- and N_2-based measurements is challenging[40,46,47] and beyond the scope of this paper.

The reduction of the internal disulfide bonds for the DRSC ions enables those ions to adopt more extended conformations and higher charge states than the corresponding DISC ions, consistent with previous results for lysozyme.[37,39] Most notably, the $\tilde{\Omega}$ value of the lowest-z ions from DRSC conditions (141.6 nm^2) is larger than the $\tilde{\Omega}$ value of the highest-z ions from DISC conditions (118.3 nm^2). This finding differs from that reported previously based on serum albumin ions generated from denaturing conditions with 5% by volume 1,2-butylene carbonate as the supercharging agent; there, many disulfide-intact and disulfide-reduced ions of a given charge state exhibited similar Ω_{N_2} values.[43] The DRSC ions display an upper charge state limit of 92+, which is 5 charges more than that for the DISC ions (Figure 1). This suggests that the inherent threshold of potential charge-sites of serum albumin is not reached by the disulfide-intact ions and that the reduction of the disulfide bonds enables additional protonation that can be attributed to the exposure of previously buried titratable sites[48] and/or greater basicities.[49]

These results show that charge-state distributions and $\tilde{\Omega}$ values of serum albumin ions in the gas phase depend on the solutions from which the proteins were ionized and how these conditions influence their structures. In the following section, we will use CAPTR to probe the relationship between the charge state and $\tilde{\Omega}$ values of charge-reduced ions.

Cation-to-Anion Proton-Transfer Reactions (CAPTR). Selected serum albumin ions generated from each of the five solution conditions were isolated and subjected to CAPTR. These ions will be denoted by "$^{\text{Condition}}P\rightarrow C$", where "Condition" represents an abbreviation for a sample condition from Table 1, "*P"* is the charge state of the precursor cation, and "*C*" is the charge state of the CAPTR product. For example, "$^{\text{DRSC}}80\rightarrow 23$" refers to the 23+ CAPTR product from the 80+ ion generated from DRSC conditions. Representative mass spectra for the $^{\text{DRSC}}80\rightarrow C$, $^{\text{DISC}}80\rightarrow C$, $^{\text{DI}}45\rightarrow C$, $^{\text{NISC}}20\rightarrow C$, and $^{\text{NI}}17\rightarrow C$ ions are shown in Figure 3. The spectra all exhibit peaks originating from a long series of CAPTR products. The relative intensities of the CAPTR products depend on experimental conditions, which has been investigated previously.[35] Peaks for *C* of at least 10 were observed for the products of ions from DRSC, DISC, and DI conditions, and peaks for *C* of at least 6 were observed for the products of ions from NISC and NI conditions. Differences in the lowest value of *C* observed for ions originating from different conditions can be attributed to the especially low mobilities of some ions and their inefficient transfer into the drift cell.

For each condition, CAPTR products originating from one to four precursor ion charge states were analyzed using IM-MS. We will first discuss general trends in the $\tilde{\Omega}$ values for the $P\rightarrow C$ ions from a given condition, and then compare results for different conditions. Figure 4A shows that the $\tilde{\Omega}$ values for the $^{\text{DRSC}}70\rightarrow C$ and $^{\text{DRSC}}80\rightarrow C$ ions depend weakly on *P* and decrease monotonically with decreasing *C* (Figure 4A). Figure 4B shows that the $\tilde{\Omega}$ values for

the $^{DISC}P\rightarrow C$, P = 50, 60, 70, and 80, ions also depend weakly on P and decrease monotonically with decreasing C. Although the $\tilde{\Omega}$ values for the $^{DI}45\rightarrow C$ ions generally decrease with decreasing C, the values for $C \approx 35$ to 40 are all similar and interrupt the monotonic decrease in $\tilde{\Omega}$ with decreasing C observed for higher and lower values of C (Figure 4C). The $\tilde{\Omega}$ values for the $^{NISC}P\rightarrow C$, P = 19 to 21, ions exhibit a large decrease after the first CAPTR event and smaller decreases for the subsequent CAPTR events, whereas the values for all $^{NISC}18\rightarrow C$ ions are similar to each other (Figure 4D). The $\tilde{\Omega}$ values for the $^{NISC}P\rightarrow C$ ions of a given C increase slightly with P, *e.g.*, the $^{NISC}P\rightarrow 14$ ions have $\tilde{\Omega}$ values of 45.3, 44.1, 43.0 and 42.2 nm^2 for P = 21, 20, 19, and 18, respectively. However, the values for all $^{NISC}P\rightarrow 6$ ions differ by less than 2.5 nm^2. Finally, the $\tilde{\Omega}$ values for the $^{NI}P\rightarrow C$, P = 15 to 17, ions are similar to each other, as well as values reported previously for the CAPTR products of these ions[38] and to values reported previously for native-like serum albumin without charge reduction (Figure 4D).[45,50] These results for the ions from NI conditions are consistent with our previous claim that the excess charges present on the native-like ions of large proteins can have a modest effect on their $\tilde{\Omega}$ values.

To aid in the direct comparison of results for ions from different conditions, Figure 4E shows the $\tilde{\Omega}$ values of the $^{DRSC}80\rightarrow C$, $^{DISC}80\rightarrow C$, $^{DI}45\rightarrow C$, $^{NISC}21\rightarrow C$, and $^{NI}17\rightarrow C$ ions. For each C, the $\tilde{\Omega}$ values for the ions from denaturing conditions are systematically larger than those for the $^{NISC}21\rightarrow C$ ions, which in turn are systematically larger than those for the $^{NI}17\rightarrow C$ ions. Among the ions from denaturing conditions, the $\tilde{\Omega}$ values of the $^{DISC}80\rightarrow C$ and $^{DI}45\rightarrow C$ ions for each C are similar to each other, except for the small difference for $C \approx 35$ to 40. By comparison, the $\tilde{\Omega}$ values of the $^{DRSC}80\rightarrow C$ are ~20 nm^2 larger for ions of large C, but those differences decrease with decreasing C. The $\tilde{\Omega}$ values from $^{DI}45\rightarrow C$, $^{DISC}80\rightarrow C$, and $^{DRSC}80\rightarrow C$ for $20 \geq C \geq 10$ ions is shown in the inset of Figure 4E, which shows that despite the decreasing differences in

$\tilde{\Omega}$ values, there are still subtle differences over this range. This suggests that these ions are still sensitive to the condensed-phase environment from which their precursor ions were generated.

The lowest-C products observed from each condition, *i.e.*, the $^{DRSC}80\rightarrow10$, $^{DISC}80\rightarrow9$, $^{DI}45\rightarrow10$, $^{NISC}21\rightarrow6$, and $^{NI}17\rightarrow6$ ion, have $\tilde{\Omega}$ values that are 66%, 61%, 50%, 15%, and 6% smaller than the values for the corresponding precursor ions, respectively. The maximum relative decreases for the CAPTR products from each of the three denaturing conditions are similar to the maximum relative decrease of 50% for $13\rightarrow3$ ions of ubiquitin from denaturing conditions,[30] of 55% for $18\rightarrow3$ ions of cytochrome *c* from denaturing conditions,[36] and of 57% for $19\rightarrow3$ ions of lysozyme from denatured, disulfide-reduced conditions.[37] However, despite the large decreases in $\tilde{\Omega}$ values for the CAPTR products from each of the three denaturing conditions, the values for the $^{DRSC}80\rightarrow10$, $^{DISC}80\rightarrow9$, and $^{DI}45\rightarrow10$ ions are all about 30% larger than those for all $^{NI}P\rightarrow C$ ions. The comparatively small maximum relative decrease for the $^{NI}17\rightarrow6$ ions is consistent with the small relative decreases reported for ions of cytochrome *c*,[36] lysozyme,[37] serum albumin, streptavidin tetramer, avidin tetramer, and alcohol dehydrogenase tetramer[38] from native-like conditions. Therefore, these results provide further support that the Ω values of native-like ions can depend only weakly on their charge state.

Although the $\tilde{\Omega}$ values of the $^{DRSC}P\rightarrow C$ ions are systematically larger than those of the corresponding $^{DISC}P\rightarrow C$ ions for high values of C, those values converge with decreasing C (Figure 4E). Therefore, the change in $\tilde{\Omega}$ values associated with each CAPTR event must be different for the ions generated from the two conditions. Figure 5 shows that for $C \geq 36$, the $\tilde{\Omega}$ values of the $^{DRSC}P\rightarrow C$ and $^{DISC}P\rightarrow C$ ions decrease on average by 1.03 and 0.95 nm^2, respectively, per CAPTR event. Both the $^{DRSC}P\rightarrow C$ and $^{DISC}P\rightarrow C$ ions exhibit greater decreases in $\tilde{\Omega}$ per CAPTR event for $C < 36$, but the average decrease for the $^{DRSC}P\rightarrow C$ ions is far greater

(~2.2 nm^2 per event) than that for the $^{DISC}P \rightarrow C$ ions (~1.5 nm^2 per event). For comparison, lysozyme ions from denatured, disulfide-reduced conditions exhibit a greater decrease in $\tilde{\Omega}$ per CAPTR event than lysozyme ions from denatured, disulfide-intact conditions;[37] the magnitude of the decreases in $\tilde{\Omega}$ per CAPTR event did not converge for the high-C ions from the two conditions. These results all suggest that the presence of disulfide bonds creates additional constraints to protein ions adopting more extended structures with increasing z and refolding to more compact structures in response to CAPTR.

Relative to NI conditions, ions from NISC conditions are generated from solutions that also contain 3% by volume sulfolane. The ions generated from NISC conditions exhibit higher charge states, larger $\tilde{\Omega}$ values, and $\tilde{\Omega}$ values that depend more strongly on z relative to those generated from NI conditions (Figures 1D, 1E, and 2). Furthermore, the $\tilde{\Omega}$ values for the $^{NISC}21 \rightarrow C$ ions of a given C are systematically larger than those of the corresponding $^{NI}17 \rightarrow C$ ions. Therefore, these results indicate that the addition of sulfolane results in structural changes that are concomitant with supercharging and that those changes are not reversed by charge reduction. In contrast, CAPTR of collisionally activated serum albumin ions from native-like conditions has been observed to result in ions with $\tilde{\Omega}$ values that are similar to those of serum albumin ions from native-like conditions that had undergone minimal activation; thus CAPTR appears to mitigate some structural changes associated with collisional activation.[38] These findings therefore support conclusions by Williams and coworkers that supercharging can disrupt the native structures of proteins and protein complexes.[51]

In addition to the $\tilde{\Omega}$ values, Figure 4 also includes two other critical values from the apparent Ω distribution, *i.e.*, 10% and 90% of the cumulative distribution function of the apparent Ω distribution as described in the *Supporting Information*. For CAPTR products of a

given *C* and solution condition, all three critical values appear to be largely independent of *P*. Note that apparent Ω distributions include contributions from gating at the beginning of and diffusion during separations,[42,52] which will be different for ions of different *z*. However, all three critical values of ions of a given *z* should be directly comparable. Quantifying these contributions and the underlying structural heterogeneity will be the subject of future studies.

These results show that the structures of CAPTR products depend on the condition from which the precursor ion was generated, the value of *C*, and to a lesser extent, the value of *P*. In the next section, we will use energy-dependent experiments to probe the potential-energy landscape for select ions to build on the relationship between Ω and *z* and potential contributions from kinetic trapping.

Conformational Landscapes of 15+ Serum Albumin. This study demonstrates that protein ions of a given charge state can be formed through multiple experimental schemes, including generation from different conditions and charge reduction via different numbers of CAPTR events. To investigate the relationship between 15+ serum albumin ions formed using three schemes, we will monitor the mobilities of these ions as a function of the injection voltage used to transfer the ions into a drift cell containing 1.2 Torr nitrogen gas. Energy deposition in these experiments will be less efficient than injection into a lower pressure, argon-filled collision cell, as used for collision-induced unfolding,[53] but more efficient than injection into a helium-filled drift cell, which occurs inadvertently in the preceding IM experiments. In this discussion, an "*" will be used to indicate the species that was activated in the experiment, *e.g.*, "$^{DISC}60\rightarrow15$*" indicates that the 15+ CAPTR product was activated during injection into the drift cell.

The structures and stabilities of the $^{NI}15$*, $^{DRSC}70\rightarrow15$*, and $^{DISC}60\rightarrow15$* ions were each probed using this strategy. The apparent Ω_{N_2} distributions of these ions are shown in Figure 6A

and the $\widetilde{\Omega}_{N_2}$ values of those distributions are plotted in Figure 6B. At the lowest injection voltage, the $\widetilde{\Omega}_{N_2}$ values of the ^{DRSC}70→15* and ^{DISC}60→15* ions are similar to each other (~64 nm^2) and much larger than that for the ^{NI}15* ions (~44 nm^2). This finding is consistent with the data in Figure 4, which were acquired with minimal activation. However, the $\widetilde{\Omega}_{N_2}$ values in Figure 6 are systematically larger than the $\widetilde{\Omega}_{He}$ values in Figure 4, which is consistent with Ω being a property of the ion-neutral pair as discussed elsewhere.[40,46,50,54] With increasing injection voltage, the $\widetilde{\Omega}_{N_2}$ values of the ^{DRSC}70→15* and ^{DISC}60→15* ions both increase to ~68 nm^2 and then decrease to values smaller than those for the ions at low energy. In contrast, the $\widetilde{\Omega}_{N_2}$ values of the ^{NI}15* ions increase with increasing injection voltage over all energies.

At the highest energies, the apparent Ω_{N_2} distributions and the corresponding $\widetilde{\Omega}_{N_2}$ values for the ^{NI}15*, ^{DRSC}70→15*, and ^{DISC}60→15* ions each appear to have largely converged and no longer depend strongly on further increases in the injection voltage. This result is consistent with each of these ions adopting a quasi-equilibrium of structures, *i.e.*, the relative population of structures depends of the relative free energies of those structures after thermalization.[30,55] The quasi-equilibrium distributions of these ions exhibit significant overlap, which suggests that these ions may share many structural motifs and are populating similar regions of their potential-energy surfaces. However, it is also possible that that these ions have isomerized to different structures that coincidently have similar mobility distributions. For example, the quasi-equilibrium Ω_{N_2} distributions of the ^{NI}15* and ^{DISC}60→15* ions are similar to each other and shifted to slightly smaller values than that for the ^{DRSC}70→15* ions. This suggests that the presence of intact disulfide bonds may preferentially favor slightly more compact structures in the gas phase, even for low-*z* ions after considerable annealing.

These results indicate that the initial structures of the $^{NI}15$, $^{DRSC}70\rightarrow15$, and $^{DISC}60\rightarrow15$ ions, *i.e.*, those present during their accumulation prior to IM, are the result of kinetic trapping and memory of their prior structures. For example, the increase in the $\widetilde{\Omega}_{N_2}$ values with increasing energy for the $^{NI}15^*$ ions can be attributed to the ions overcoming isomerization barriers to more extended structures that minimize Coulombic repulsion between the excess charges, likely at the expense of other intramolecular interactions that were present in the initial, kinetically trapped structure. In contrast, the decrease in the $\widetilde{\Omega}_{N_2}$ values with increasing energy for the $^{DRSC}70\rightarrow15^*$ and $^{DISC}60\rightarrow15^*$ ions can be attributed to the ions overcoming isomerization barriers to more compact structures that include more favorable intramolecular interactions that were not present in the initial structures adopted after CAPTR of the highly charged precursor ions. Therefore, activation of these ions from very different conditions may enable access to similar regions of the potential energy landscape. These results complement a growing body of literature reporting that although many elements of condensed-phase structure can be preserved in the gas phase,[24] fidelity is the result of kinetic trapping and gas-phase protein ions at equilibrium may have vastly different structures.[56,57]

Conclusions

These experiments used CAPTR, IM, and post-CAPTR activation to explore the relationship between the $\tilde{\Omega}$ and z values of serum albumin ions generated from five conditions that retain varying degrees of the native structure (Table 1). Ions generated from increasingly disruptive conditions exhibited higher charge states and larger $\tilde{\Omega}$ values (Figures 1 and 2). CAPTR of selected precursor ions from each condition showed that the $\tilde{\Omega}$ values of the product ions depend on the original solution conditions, and to varying extents, the charge state of the

product and precursor ions. The $\tilde{\Omega}$ values of the CAPTR products of the ions from NISC conditions are systematically larger than those from NI conditions, and both depend weakly on C (Figure 4D). At high C, the $\tilde{\Omega}$ values of the CAPTR products of the ions generated from DRSC, DISC, and DI conditions depend strongly on both C and the presence of disulfide bonds (Figure 4). With decreasing C, the differences between the $\tilde{\Omega}$ values of the disulfide-intact and disulfide-reduced ions from these conditions decrease (Figure 4E), although small differences are still observed (Figure 4E, inset). This is a consequence of the change in the $\tilde{\Omega}$ value per CAPTR event being greater for the $^{DRSC}P \rightarrow C$ ions (2.2 nm^2) than for the $^{DISC}P \rightarrow C$ ions (1.5 nm^2) for $C <$ 36, even though both ions exhibit an ~1.0 nm^2 decrease in $\tilde{\Omega}$ values per CAPTR event for larger C (Figure 5). More generally, these results are consistent with disulfide bonds preventing extension to larger structures at high z, as well as preventing isomerization to more compact structures at low z.

The stability of 15+ ions produced from three different origins was examined using post-CAPTR activation of the $^{DRSC}70 \rightarrow 15^*$, $^{DISC}60 \rightarrow 15^*$, and $^{NI}15^*$ ions. At low injection voltages, the denatured ions have $\tilde{\Omega}$ values that are significantly larger than those for the native-like ion. At high injection voltages, the three ions have converged to Ω distributions that have significant overlap, especially for the $^{DISC}60 \rightarrow 15^*$ and $^{NI}15^*$ ions. This is consistent with these ions sharing structural motifs and accessing similar regions of the potential-energy surface. Additionally, the $\tilde{\Omega}$ value of the $^{DRSC}70 \rightarrow 15^*$ and $^{DISC}60 \rightarrow 15^*$ ions becomes largely independent of the injection voltage above 45 V, consistent with these ions adopting a quasi-equilibrium of structures.

These results provided new insights into the relationship between the structures, charge states, and solution conditions of a large, multi-domain protein in the gas phase. Whereas the $\tilde{\Omega}$ values of low-z CAPTR products of small proteins from denaturing conditions are similar to

those for the corresponding native-like ions, the low-*z* CAPTR products of serum albumin are at least 30% larger than those for the native-like ions of serum albumin. This large difference can be understood in the context of the energy-dependent experiments. Relative to the structures formed after significant annealing, the CAPTR products of the ions from denaturing conditions have significantly larger $\tilde{\Omega}$ values and the ions from native-like conditions have significantly smaller $\tilde{\Omega}$ values (Figure 6). Together, these results show that the structures of the original ions from electrospray ionization and their CAPTR products all depend strongly on the original solution condition and are a consequence of kinetic trapping. Therefore, CAPTR and energy-dependent IM provide many complementary probes that are sensitive to the higher-order structures and disulfide bonding of proteins, which may be useful for biotherapeutic characterization.

ASSOCIATED CONTENT

Supporting Information. Supporting Information Available: This material is available free of charge via the Internet at http://pubs.acs.org.

Protocol for reduction/alkylation of cysteine residues, determination of Ω values from arrival-time distributions, calculation of Ω values for models of serum albumin and comparison to experimental Ω values, Table S1, Figure S1, and Figure S2

AUTHOR INFORMATION

Corresponding Author

*E-mail: mattbush@uw.edu

ACKNOWLEDGEMENTS

This material is based upon work supported by the National Science Foundation under CHE–1807382 (M. F. B.).

References

(1) Fersht, A. R. From the First Protein Structures to Our Current Knowledge of Protein Folding: Delights and Scepticisms. *Nat. Rev. Mol. Cell Biol.* **2008**, *9*, 650–654.

(2) Carter, P. J. Introduction to Current and Future Protein Therapeutics: A Protein Engineering Perspective. *Exp. Cell Res.* **2011**, *317*, 1261–1269.

(3) Bale, J. B.; Gonen, S.; Liu, Y.; Sheffler, W.; Ellis, D.; Thomas, C.; Cascio, D.; Yeates, T. O.; Gonen, T.; King, N. P.; et al. Accurate Design of Megadalton-Scale Two-Component Icosahedral Protein Complexes. *Science* **2016**, *353*, 389–394.

(4) Hsia, Y.; Bale, J. B.; Gonen, S.; Shi, D.; Sheffler, W.; Fong, K. K.; Nattermann, U.; Xu, C.; Huang, P.-S.; Ravichandran, R.; et al. Design of a Hyperstable 60-Subunit Protein Icosahedron. *Nature* **2016**, *535*, 136–139.

(5) Brange, J.; Ribel, U.; Hansen, J. F.; Dodson, G.; Hansen, M. T.; Havelund, S.; Melberg, S. G.; Norris, F.; Norris, K.; Snel, L.; et al. Monomeric Insulins Obtained by Protein Engineering and Their Medical Implications. *Nature* **1988**, *333*, 679-682.

(6) Walsh, G.; Jefferis, R. Post-Translational Modifications in the Context of Therapeutic Proteins. *Nat. Biotechnol.* **2006**, *24*, 1241-1252.

(7) Walsh, G. Protein Engineering: Case Studies of Commercialized Engineered Products. *Biochem. Mol. Biol. Educ.* **2007**, *35*, 2–8.

(8) Pastore, A. New Challenges in Structural Biology: Catching the Complexity of Dynamic Nanomachines. *Front. Mol. Biosci.* **2014**, *1*, doi:10.3389/fmolb.2014.00003

(9) Rosati, S.; Yang, Y.; Barendregt, A.; Heck, A. J. R. Detailed Mass Analysis of Structural Heterogeneity in Monoclonal Antibodies Using Native Mass Spectrometry. *Nat. Protoc.* **2014**, *9*, 967–976.

(10) Slabinski, L.; Jaroszewski, L.; Rodrigues, A. P. C.; Rychlewski, L.; Wilson, I. A.; Lesley, S. A.; Godzik, A. The Challenge of Protein Structure Determination—lessons from Structural Genomics. *Protein Sci.* **2007**, *16*, 2472–2482.

(11) Liko, I.; Allison, T. M.; Hopper, J. T.; Robinson, C. V. Mass Spectrometry Guided Structural Biology. *Curr. Opin. Struct. Biol.* **2016**, *40*, 136–144.

(12) Beavis, R. C.; Chait, B. T. High-Accuracy Molecular Mass Determination of Proteins Using Matrix-Assisted Laser Desorption Mass Spectrometry. *Anal. Chem.* **1990**, *62*, 1836–1840.

(13) Olsen, J. V.; de Godoy, L. M. F.; Li, G.; Macek, B.; Mortensen, P.; Pesch, R.; Makarov, A.; Lange, O.; Horning, S.; Mann, M. Parts per Million Mass Accuracy on an Orbitrap Mass Spectrometer via Lock Mass Injection into a C-Trap. *Mol Cell Proteomics* **2005**, *4*, 2010–2021.

(14) Taverner, T.; Hernández, H.; Sharon, M.; Ruotolo, B. T.; Matak-Vinković, D.; Devos, D.; Russell, R. B.; Robinson, C. V. Subunit Architecture of Intact Protein Complexes from Mass Spectrometry and Homology Modeling. *Acc. Chem. Res.* **2008**, *41*, 617–627.

(15) Gahoual, R.; Heidenreich, A.-K.; Somsen, G. W.; Bulau, P.; Reusch, D.; Wuhrer, M.; Haberger, M. Detailed Characterization of Monoclonal Antibody Receptor Interaction Using Affinity Liquid Chromatography Hyphenated to Native Mass Spectrometry. *Anal. Chem.* **2017**, *89*, 5404–5412.

(16) Hernández, H.; Robinson, C. V. Determining the Stoichiometry and Interactions of Macromolecular Assemblies from Mass Spectrometry. *Nat. Protoc.* **2007**, *2*, 715–726.

(17) Aquilina, J. A.; Benesch, J. L. P.; Bateman, O. A.; Slingsby, C.; Robinson, C. V. Polydispersity of a Mammalian Chaperone: Mass Spectrometry Reveals the Population of Oligomers in αB-Crystallin. *Proc. Natl. Acad. Sci.* **2003**, *100*, 10611–10616.
(18) Lanucara, F.; Holman, S. W.; Gray, C. J.; Eyers, C. E. The Power of Ion Mobility-Mass Spectrometry for Structural Characterization and the Study of Conformational Dynamics. *Nat. Chem.* **2014**, *6*, 281–294.
(19) Gabelica, V.; Marklund, E. Fundamentals of Ion Mobility Spectrometry. *Curr. Opin. Chem. Biol.* **2018**, *42*, 51–59.
(20) Loo, J. A.; Berhane, B.; Kaddis, C. S.; Wooding, K. M.; Xie, Y.; Kaufman, S. L.; Chernushevich, I. V. Electrospray Ionization Mass Spectrometry and Ion Mobility Analysis of the 20S Proteasome Complex. *J. Am. Soc. Mass Spectrom.* **2005**, *16*, 998–1008.
(21) Hall, Z.; Politis, A.; Robinson, C. V. Structural Modeling of Heteromeric Protein Complexes from Disassembly Pathways and Ion Mobility-Mass Spectrometry. *Structure* **2012**, *20*, 1596–1609.
(22) Heck, A. J. R. Native Mass Spectrometry: A Bridge between Interactomics and Structural Biology. *Nat. Methods* **2008**, *5*, 927–933.
(23) Meyer, T.; Gabelica, V.; Grubmüller, H.; Orozco, M. Proteins in the Gas Phase. *Wiley Interdiscip. Rev. Comput. Mol. Sci.* **2013**, *3*, 408–425.
(24) Seo, J.; Hoffmann, W.; Warnke, S.; Bowers, M. T.; Pagel, K.; von Helden, G. Retention of Native Protein Structures in the Absence of Solvent: A Coupled Ion Mobility and Spectroscopic Study. *Angew. Chem. Int.* **2016**, *55*, 14173–14176.
(25) Barney, B. L.; Pratt, S. N.; Austin, D. E. Survivability of Bare, Individual Bacillus Subtilis Spores to High-Velocity Surface Impact: Implications for Microbial Transfer through Space. *Planet. Space Sci.* **2016**, *125*, 20–26.
(26) Bohrer, B. C.; Merenbloom, S. I.; Koeniger, S. L.; Hilderbrand, A. E.; Clemmer, D. E. Biomolecule Analysis by Ion Mobility Spectrometry. *Annu. Rev. Anal. Chem.* **2008**, *1*, 293–327.
(27) Wyttenbach, T.; Bowers, M. T. Structural Stability from Solution to the Gas Phase: Native Solution Structure of Ubiquitin Survives Analysis in a Solvent-Free Ion Mobility–Mass Spectrometry Environment. *J. Phys. Chem. B* **2011**, *115*, 12266–12275.
(28) Jarrold, M. F. Unfolding, Refolding, and Hydration of Proteins in the Gas Phase. *Acc. Chem. Res.* **1999**, *32*, 360–367.
(29) Zhao, Q.; Schieffer, G. M.; Soyk, M. W.; Anderson, T. J.; Houk, R. S.; Badman, E. R. Effects of Ion/ion Proton Transfer Reactions on Conformation of Gas-Phase Cytochrome c Ions. *J. Am. Soc. Mass Spectrom.* **2010**, *21*, 1208–1217.
(30) Laszlo, K. J.; Munger, E. B.; Bush, M. F. Folding of Protein Ions in the Gas Phase after Cation-to-Anion Proton-Transfer Reactions. *J. Am. Chem. Soc.* **2016**, *138*, 9581–9588.
(31) Lermyte, F.; Łącki, M. K.; Valkenborg, D.; Gambin, A.; Sobott, F. Conformational Space and Stability of ETD Charge Reduction Products of Ubiquitin. *J. Am. Soc. Mass Spectrom.* **2017**, *28*, 69–76.
(32) McLuckey, S. A.; Stephenson, J. L. Ion/ion Chemistry of High-Mass Multiply Charged Ions. *Mass Spectrom. Rev.* **1998**, *17*, 369–407.
(33) McLuckey, S. A.; Huang, T.-Y. Ion/Ion Reactions: New Chemistry for Analytical MS. *Anal. Chem.* **2009**, *81*, 8669–8676.

(34) Lermyte, F.; Konijnenberg, A.; Williams, J. P.; Brown, J. M.; Valkenborg, D.; Sobott, F. ETD Allows for Native Surface Mapping of a 150 kDa Noncovalent Complex on a Commercial Q-TWIMS-TOF Instrument. *J. Am. Soc. Mass Spectrom.* **2014**, *25*, 343–350.
(35) Laszlo, K. J.; Bush, M. F. Analysis of Native-Like Proteins and Protein Complexes Using Cation to Anion Proton Transfer Reactions (CAPTR). *J. Am. Soc. Mass Spectrom.* **2015**, *26*, 2152–2161.
(36) Laszlo, K. J.; Buckner, J. H.; Munger, E. B.; Bush, M. F. Native-Like and Denatured Cytochrome *c* Ions Yield Cation-to-Anion Proton Transfer Reaction Products with Similar Collision Cross-Sections. *J. Am. Soc. Mass Spectrom.* **2017**, *28*, 1382–1391.
(37) Laszlo, K. J.; Munger, E. B.; Bush, M. F. Effects of Solution Structure on the Folding of Lysozyme Ions in the Gas Phase. *J. Phys. Chem. B* **2017**, *121*, 2759–2766.
(38) Laszlo, K. J.; Bush, M. F. Interpreting the Collision Cross Sections of Native-like Protein Ions: Insights from Cation-to-Anion Proton-Transfer Reactions. *Anal. Chem.* **2017**, *89*, 7607–7614.
(39) Valentine, S. J.; Anderson, J. G.; Ellington, A. D.; Clemmer, D. E. Disulfide-Intact and -Reduced Lysozyme in the Gas Phase: Conformations and Pathways of Folding and Unfolding. *J. Phys. Chem. B* **1997**, *101*, 3891–3900.
(40) Canzani, D.; Laszlo, K. J.; Bush, M. F. Ion Mobility of Proteins in Nitrogen Gas: Effects of Charge State, Charge Distribution, and Structure. *J. Phys. Chem. A* **2018**, *122*, 5625-5634.
(41) Williams, J. P.; Brown, J. M.; Campuzano, I.; Sadler, P. J. Identifying Drug Metallation Sites on Peptides Using Electron Transfer Dissociation (ETD), Collision Induced Dissociation (CID) and Ion Mobility-Mass Spectrometry (IM-MS). *Chem. Commun.* **2010**, *46*, 5458–5460.
(42) Allen, S. J.; Giles, K.; Gilbert, T.; Bush, M. F. Ion Mobility Mass Spectrometry of Peptide, Protein, and Protein Complex Ions Using a Radio-Frequency Confining Drift Cell. *Analyst* **2016**, *141*, 884–891.
(43) Donor, M. T.; Ewing, S. A.; Zenaidee, M. A.; Donald, W. A.; Prell, J. S. Extended Protein Ions Are Formed by the Chain Ejection Model in Chemical Supercharging Electrospray Ionization. *Anal. Chem.* **2017**, *89*, 5107–5114.
(44) Allen, S. J. Development of Ion Mobility Mass Spectrometry Instrumentation to Investigate the Gas-Phase Structures of Protein and Protein Complex Ions. Thesis, 2017.
(45) Allen, S. J.; Schwartz, A. M.; Bush, M. F. Effects of Polarity on the Structures and Charge States of Native-like Proteins and Protein Complexes in the Gas Phase. *Anal. Chem.* **2013**, *85*, 12055–12061.
(46) Bleiholder, C.; Johnson, N. R.; Contreras, S.; Wyttenbach, T.; Bowers, M. T. Molecular Structures and Ion Mobility Cross Sections: Analysis of the Effects of He and N2 Buffer Gas. *Anal. Chem.* **2015**, *87*, 7196–7203.
(47) May, J. C.; Goodwin, C. R.; Lareau, N. M.; Leaptrot, K. L.; Morris, C. B.; Kurulugama, R. T.; Mordehai, A.; Klein, C.; Barry, W.; Darland, E.; et al. Conformational Ordering of Biomolecules in the Gas Phase: Nitrogen Collision Cross Sections Measured on a Prototype High Resolution Drift Tube Ion Mobility-Mass Spectrometer. *Anal. Chem.* **2014**, *86*, 2107–2116.
(48) Loo, R. R. O.; Lakshmanan, R.; Loo, J. A. What Protein Charging (and Supercharging) Reveal about the Mechanism of Electrospray Ionization. *J. Am. Soc. Mass Spectrom.* **2014**, *25*, 1675–1693.

(49) Zenaidee, M. A.; Leeming, M. G.; Zhang, F.; Funston, T. T.; Donald, W. A. Highly Charged Protein Ions: The Strongest Organic Acids to Date. *Angew. Chem. Int. Ed.* **2017**, *56*, 8522–8526.
(50) Bush, M. F.; Hall, Z.; Giles, K.; Hoyes, J.; Robinson, C. V.; Ruotolo, B. T. Collision Cross Sections of Proteins and Their Complexes: A Calibration Framework and Database for Gas-Phase Structural Biology. *Anal. Chem.* **2010**, *82*, 9557–9565.
(51) Sterling, H. J.; Prell, J. S.; Cassou, C. A.; Williams, E. R. Protein Conformation and Supercharging with DMSO from Aqueous Solution. *J. Am. Soc. Mass Spectrom.* **2011**, *22*, 1178–1186.
(52) Davidson, K. L.; Bush, M. F. Effects of Drift Gas Selection on the Ambient-Temperature, Ion Mobility Mass Spectrometry Analysis of Amino Acids. *Anal. Chem.* **2017**, *89*, 2017–2023.
(53) Eschweiler, J. D.; Martini, R. M.; Ruotolo, B. T. Chemical Probes and Engineered Constructs Reveal a Detailed Unfolding Mechanism for a Solvent-Free Multidomain Protein. *J. Am. Chem. Soc.* **2017**, *139*, 534–540.
(54) Lee, J. W.; Lee, H. H. L.; Davidson, K. L.; Bush, M. F.; Kim, H. I. Structural Characterization of Small Molecular Ions by Ion Mobility Mass Spectrometry in Nitrogen Drift Gas: Improving the Accuracy of Trajectory Method Calculations. *Analyst* **2018**, *143*, 1786–1796.
(55) Pierson, N. A.; Valentine, S. J.; Clemmer, D. E. Evidence for a Quasi-Equilibrium Distribution of States for Bradykinin [M + 3H]3+ Ions in the Gas Phase. *J. Phys. Chem. B* **2010**, *114*, 7777–7783.
(56) Breuker, K.; McLafferty, F. W. Stepwise Evolution of Protein Native Structure with Electrospray into the Gas Phase, 10^{-12} to 10^{2} s. *Proc. Natl. Acad. Sci.* **2008**, *105*, 18145–18152.
(57) Allen, S. J.; Eaton, R. M.; Bush, M. F. Structural Dynamics of Native-Like Ions in the Gas Phase: Results from Tandem Ion Mobility of Cytochrome c. *Anal. Chem.* **2017**, *89*, 7527–7534.

Table 1. Solution Conditions

	DSB Intact	Description	Solvent and Additives (by volume)	z_{min}	z_{max}
DRSC	No[a]	denaturing, supercharging	1:1 water:acetonitrile with 0.1% trifluoroacetic acid and 15% propylene carbonate	53	92
DISC	Yes	denaturing, supercharging	water with 15% propylene carbonate and 0.5% acetic acid	34	87
DI	Yes	denaturing	70:30 water:methanol with 0.2% formic acid	26	56
NISC	Yes	native-like, supercharging	aqueous 200 mM ammonium acetate at pH 7 with 3% sulfolane	15	26
NI	Yes	native-like	aqueous 200 mM ammonium acetate at pH 7	14	17

[a] Prior to preparation of the electrospray solution, the protein sample was reduced and alkylated as described in the *Supporting Information*.

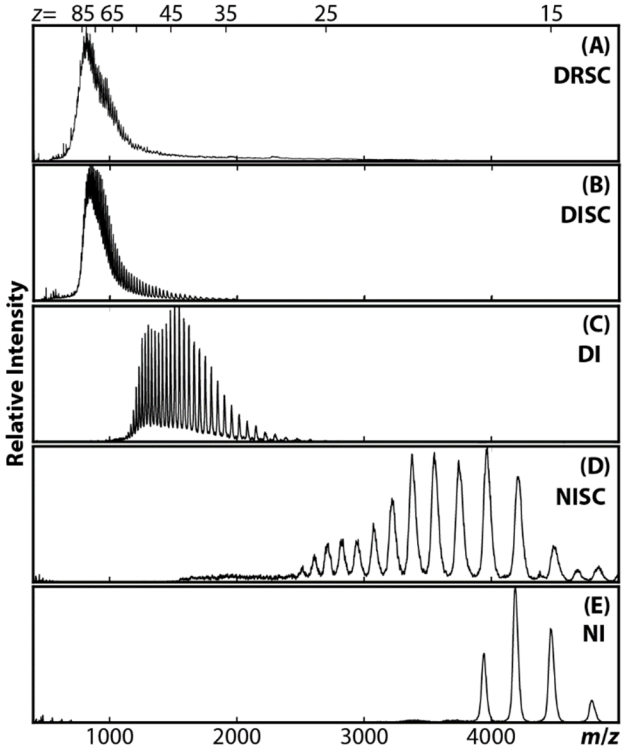

Figure 1. Representative mass spectra of serum albumin generated from each solution condition described in Table 1, as labeled in each panel. Values along the top axis correspond to the charge state assignments for panels B-E. Relative to the ions from the other conditions, the *m*/*z* values for the DRSC ions are shifted due to alkylation following reduction of the disulfide bonds. Note that as ions become larger and more highly charged, scattering during time-of-flight analysis becomes increasingly likely.

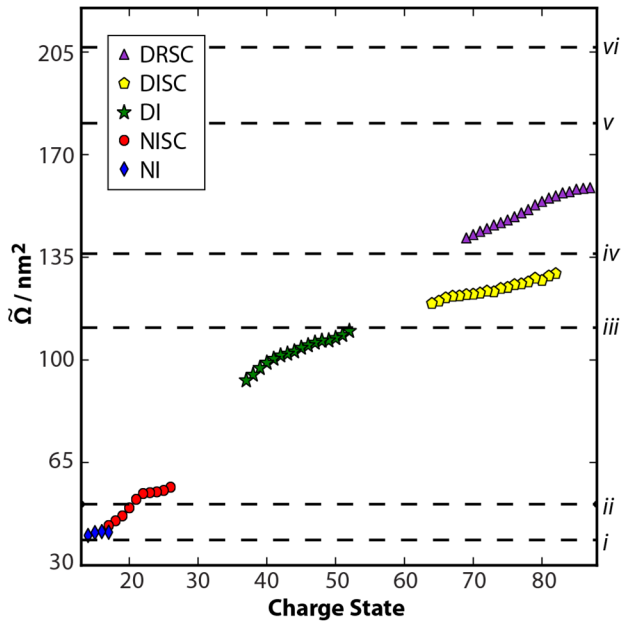

Figure 2. $\tilde{\Omega}$ values for a subset of the ions generated from each of the five solution conditions determined using a field-dependent method, as described in the *Supporting Information*. Note that all $\tilde{\Omega}$ values are with helium gas, unless otherwise noted. Black dashed lines correspond to Ω values calculated for the native (*i* and *ii*, for the projection approximation and exact hard sphere scattering methods, respectively), the α-helical (*iii* and *iv*), and the linear (*v* and *vi*) models of serum albumin. Details of the methods and rationale for the calculations are described in the *Supporting Information.*

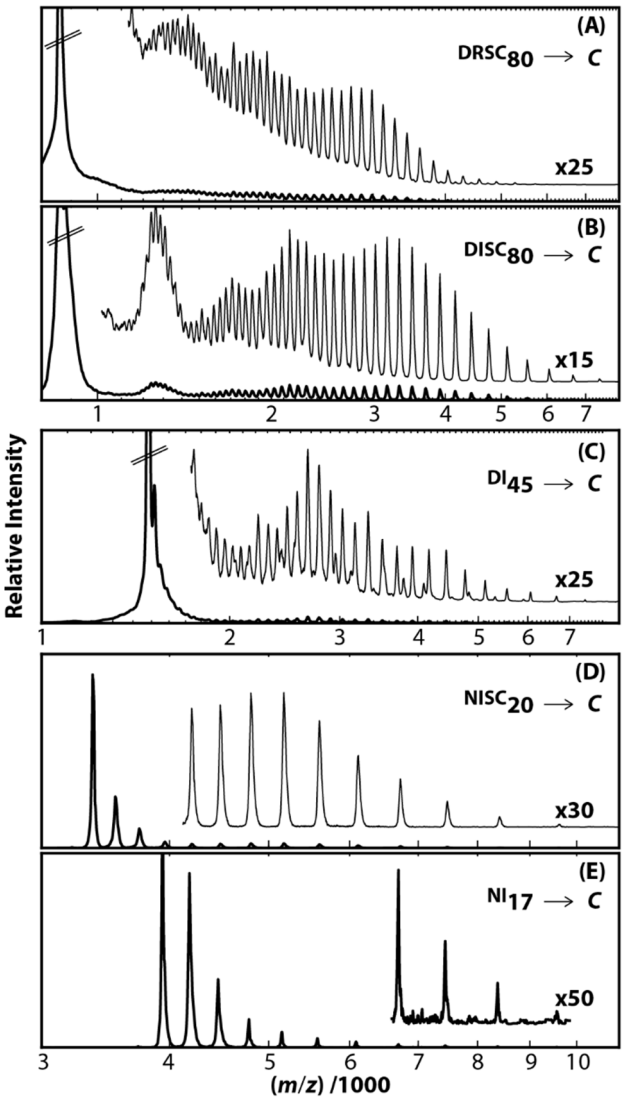

Figure 3. CAPTR mass spectra of the $^{DRSC}80\rightarrow C$, $^{DISC}80\rightarrow C$, $^{DI}45\rightarrow C$, $^{NISC}20\rightarrow C$, and $^{NI}17\rightarrow C$ ions. The identities of ions are indicated by "$^{Condition}P\rightarrow C$", where "Condition" is an abbreviation from Table 1, "*P"* is the charge state of the precursor cation, and "*C*" is the charge state of the CAPTR product. Selected regions of each spectrum have been amplified as indicated and offset from the horizontal axis to aid in visualization.

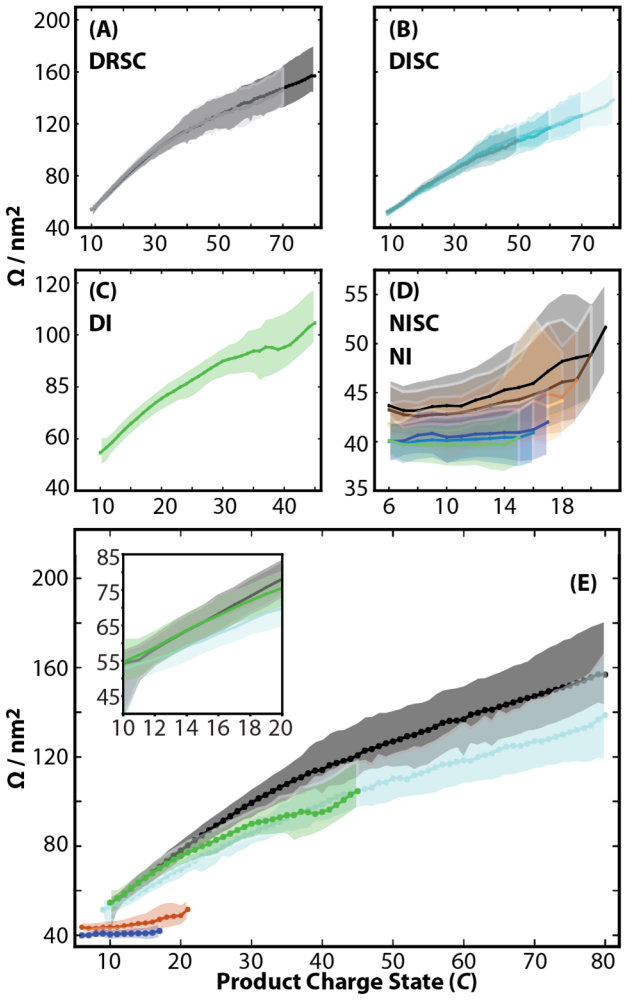

Figure 4. Results from IM-MS of the CAPTR products. Markers correspond to the $\tilde{\Omega}$ values and the shaded regions span from 10% to 90% of the cumulative distribution function of each apparent Ω distribution, as described in the *Supporting Information*. Results for (A) the $^{DRSC}P \rightarrow C$, P = 70 and 80, ions, (B) the $^{DISC}P \rightarrow C$, P = 50, 60, 70, and 80, ions, (C) the $^{DI}45 \rightarrow C$ ions, and (D) the $^{NISC}P \rightarrow C$, P = 18 to 21 (*copper tones*), and the $^{NI}P \rightarrow C$, P = 15 to 17 (*cool tones*), ions. (E) Summary of results for the highest P from each solution condition, *i.e.*, the $^{DRSC}80 \rightarrow C$, $^{DISC}80 \rightarrow C$, $^{DI}45 \rightarrow C$, $^{NISC}21 \rightarrow C$, and $^{NI}17 \rightarrow C$ ions. The inset of E shows the results for $^{DRSC}80 \rightarrow C$, $^{DISC}80 \rightarrow C$, $^{DI}45 \rightarrow C$ ions for $20 \geq C \geq 10$.

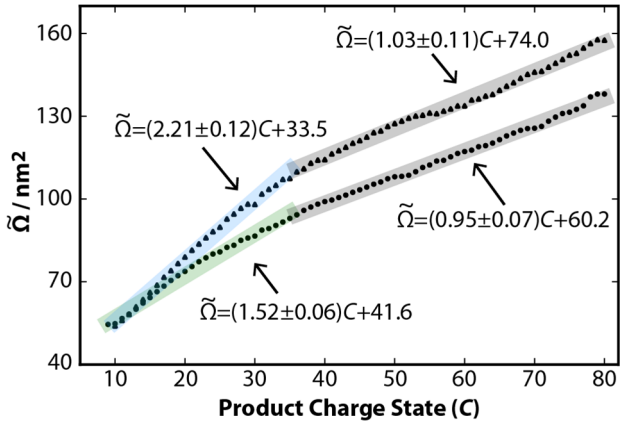

Figure 5. $\tilde{\Omega}$ values of the $^{DISC}P \rightarrow C$ (*circles*, average of results for P = 50, 60, 70, and 80) and $^{DRSC}P \rightarrow C$ (*triangles*, average of results for P = 80 and 70), as a function of C. The transparent lines correspond to the line of best-fit and spans the range of C used for the linear regression. Although the $\tilde{\Omega}$ values for the $^{DRSC}P \rightarrow C$ ions are systematically larger than the corresponding $^{DISC}P \rightarrow C$ ions, both exhibit similar changes in $\tilde{\Omega}$ per CAPTR event for $C \geq 36$ (~1.0 nm^2 per event, *gray lines*). In contrast, for $C < 36$ the change in $\tilde{\Omega}$ per CAPTR event for the $^{DRSC}P \rightarrow C$ ions is far greater (~2.2 nm^2 per event, *cyan line*) than that for the $^{DISC}P \rightarrow C$ ions (~1.5 nm^2 per event, *green line*).

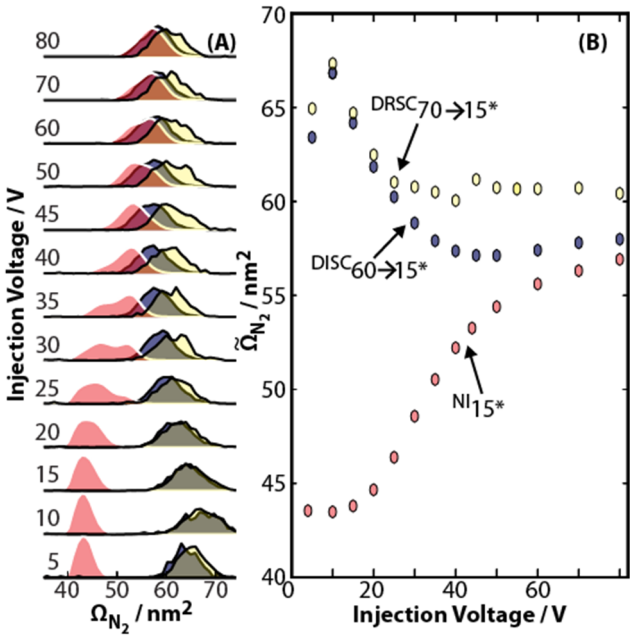

Figure 6. (A) Apparent Ω_{N_2} distributions of the ^{NI}15* (*magenta*), ^{DISC}60→15* (*purple*), and ^{DISC}70→15* (*yellow*) ions as a function of the injection voltage used to transfer the ions into a drift cell containing 1.2 Torr nitrogen gas. (B) $\tilde{\Omega}_{N_2}$ values of the distributions in panel A as a function of the injection voltage.

TOC Graphic

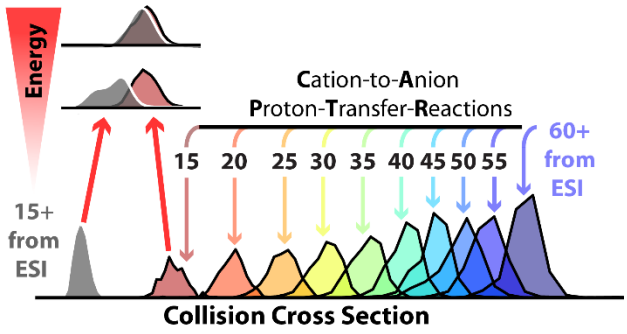
Energy
Cation-to-Anion
Proton-Transfer-Reactions
15 20 25 30 35 40 45 50 55
60+
from
ESI
15+
from
ESI
Collision Cross Section